Publications of the Astronomical Society of Japan, 2025, **77**(4), 678–686
https://doi.org/10.1093/pasj/psaf033
Advance access publication date: 2025 May 22

Measuring the kinematic motion of Cygnus X-3: Support for high peculiar velocity

Jeong-Sook Kim,[1,2,3,*] **Nobuyuki Sakai,**[4,5] **Soon-Wook Kim,**[3,*] **Tomoaki Oyama,**[5] **Kazuya Hachisuka,**[5] **and Kimitake Hayasaki**[2,6,7]

[1]National Astronomical Observatories, Chinese Academy of Sciences, Beijing 100012, China
[2]Department of Astronomy and Space Science, Chungbuk National University, Cheongju 361-763, Republic of Korea
[3]Korea Astronomy and Space Science Institute, 776 Daedeok-daero, Yuseong-gu, Daejeon 34055, Republic of Korea
[4]National Astronomical Research Institute of Thailand (Public Organization), 260 Moo 4, T. Donkaew, A. Maerim, Chiang Mai 50180, Thailand
[5]Mizusawa VLBI Observatory, National Astronomical Observatory of Japan, 2-12 Hoshiga-oka, Mizusawa, Oshu-shi, Iwate 023-0861, Japan
[6]Harvard-Smithsonian Center for Astrophysics, 60 Garden Street, Cambridge, MA 02138, USA
[7]Department of Physical Sciences, Aoyama Gakuin University, 5-10-1 Fuchinobe, Chuo-ku, Sagamihara, Kanagawa 252-5258, Japan
*Email: evony08@gmail.com, skim@kasi.re.kr

Abstract

We carry out astrometric Very Long Baseline Interferometry (VLBI) observations for Cygnus X-3, a high-mass X-ray binary (HMXB), with the Korean–Japanese joint VLBI array (KaVA) from 2020 to 2021. The observations have been optimized for the subdued phase when Cygnus X-3 is relatively faint, sidestepping a giant flare between 2020 and 2021. The position of the core in Cygnus X-3 was measured through the observations. Based on accumulating core positions from the available archival data, obtained over ∼38 yr with the Very Large Array (VLA), the Very Long Baseline Array (VLBA), and the European VLBI Network (EVN), in addition to our KaVA observations, we estimated the proper motion components to be $\mu_\alpha \cos\delta = -2.720 \pm 0.019$ mas yr^{-1} and $\mu_\delta = -3.693 \pm 0.019$ mas yr^{-1} in RA and Dec, and $\mu_l \cos b = -4.587 \pm 0.027$ mas yr^{-1} and $\mu_b = -0.001 \pm 0.004$ mas yr^{-1} in galactic longitude and galactic latitude, respectively. The proper motion results are in good agreement with previous results. Furthermore, the uncertainties we obtained are reduced by a factor of 3. The proper motion measurement allows us to constrain the peculiar velocity of the system in three-dimensional space to be 292 ± 127 km s^{-1} with 1σ error. Based on the correlation between the orbital period and the peculiar velocity in HMXBs, a peculiar velocity with an orbital period of 0.2 d, like that of Cygnus X-3, is expected to be higher than 100 km s^{-1} within 1σ error. This suggests the possibility that the compact star probably received a substantial kick during its birth, most likely caused by a supernova explosion rather than a direct collapse.

Keywords: binaries: close — binaries: general — radio continuum: stars — X-rays: binaries

1 Introduction

High-mass X-ray binaries (HMXBs) are systems where a compact object—either a black hole (BH) or a neutron star (NS)—is gravitationally bound mainly to a massive O- or B-type star with a mass greater than 8 $M_\odot$ as a companion. The compact object accretes material from the companion star, and forms through the gravitational collapse of a massive star during a supernova explosion, resulting in either a BH or an NS (Brandt & Podsiadlowski 1995; Vanbeveren et al. 2020). At the moment of the supernova, the remnant compact object can receive an additional acceleration, known as the natal kick, which has a significant impact on its subsequent motion. Because the massive companion stars in HMXBs have short lifespans, HMXBs are considered to be young systems. Consequently, the current positions and kinematics of HMXBs are strongly influenced by this natal kick, along with the velocity imparted to the binary during its formation, linking supernova mechanisms to the observed dynamics of compact objects.

We focus on the mysterious HMXB system, Cygnus X-3, which consists of an unidentified compact object and a rare type of companion, a Wolf–Rayet companion (van Kerkwijk et al. 1996; Koch-Miramond et al. 2002). The nature of the unidentified compact object is considered to be a BH or an NS, depending on the assumed distance and mass of the companion (Koljonen & Maccarone 2017). Cygnus X-3 is also one of only a few strong TeV gamma-ray sources among microquasars, first discovered by Mori et al. (1997), and later confirmed with the Fermi Large Area Telescope (Fermi LAT Collaboration 2009) and AGILE (Tavani et al. 2009). After its discovery in the X-ray band by Giacconi et al. (1967), Cygnus X-3 has been actively observed in the radio, infrared, X-ray, and gamma-ray. It has a short orbital period of 4.8 h in X-ray and infrared (Bhargava et al. 2017), and it has displayed the most frequent flaring activity in the radio among microquasars, from a few tens of minutes to over 10 d (Gregory et al. 1972; Waltman et al. 1996).

Such flares have been detected at multiwavelengths in the radio, infrared, X-ray, and gamma-ray. In particular, based on the relation between X-ray and radio behaviors along the cycle of a jet ejection, Koljonen et al. (2010) divided states associated with the flaring activity into a few states such as the hypersoft state, the flaring soft X-ray state, the flaring intermediate state, the flaring hard X-ray state, the transition state, and the quiescent state. The jet ejection typically occurs at the transition from the hypersoft state to the flaring soft X-ray state. Therefore, a giant flaring activity is initially quenched to a level of a few mJy, and a rapid rise of two to

Received: 2024 May 21; **Accepted:** 2025 March 25

three orders of magnitude follows to peak up to over 10 Jy within a few days (Waltman et al. 1996; Trushkin et al. 2017). Cygnus X-3 has undergone its giant outbursts sporadically with an irregular interval of a few months to years. A handful of VLBI observations during its giant flares have revealed that the relativistic jets eject predominantly aligned in a north–south direction (Mioduszewski et al. 2001; Miller-Jones et al. 2004; Tudose et al. 2007; Kim et al. 2013; Egron et al. 2017).

Cygnus X-3 is located in the Galactic plane, and therefore the extinction towards the source is high ($A_V \sim 30$ mag) (Ogley et al. 2001). The Wolf–Rayet companion has been estimated to have a visual magnitude of $V = 29 \pm 1$, and has not been detected in the optical Digitized Sky Survey (Wagner et al. 1990; Ogley et al. 2001). Accordingly, it has not been possible to measure the distance—an essential parameter to determine the physical and kinematical characteristics of the system, such as the space velocity and mass—using optical observations (e.g., Gaia). An alternative way to measure the distance would be through VLBI observations, particularly because Cygnus X-3 is a persistent radio source. However, the VLBI parallax measurement of Cygnus X-3 had been prevented due to the strong scattering along the line of sight to Cygnus X-3 (Mioduszewski et al. 2001). Recently, measurements of the parallax for Cygnus X-3 have been successful using VLBA observations at 43 GHz by Reid and Miller-Jones (2023), and the estimated distance based on the parallax is $9.67^{+0.53}_{-0.48}$ kpc. Therefore, based on the updated distance, we tried to constrain the intrinsic velocity range to deduce the mechanism of birth for the compact object in Cygnus X-3.

In this paper, we present a more accurate proper motion measurement of the moving core of Cygnus X-3, after adding the first astrometric observations using KaVA1, the Korean–Japanese joint VLBI array during 2020–2021. In section 4, we describe our KaVA observations and estimate the peculiar velocity of Cygnus X-3 based on its three-dimensional kinematics. In section 3, we compare the peculiar motion of Cygnus X-3 with other HMXBs containing BH and NS accretors. The summary and conclusion are presented in section 4.

2 Observations and results

2.1 VLBI observations with KaVA

Cygnus X-3 was observed twice, on 2020 October 19 (MJD 59141) and 2021 May 9 (MJD 59343) with the KaVA. The fast switching mode was adopted for both a phase reference source J2007+4029 and Cygnus X-3 with a separation angle of 4.°9. J2007+4029 and Cygnus X-3 were observed alternately for 20 and 30 s, respectively. A bandpass calibrator J2015+4032 was also observed every 70–90 min in each observation. With the VLBI Exploration of Radio Astrometry (VERA), we could not use its usual two-beam observational mode, in which the atmospheric correction can be improved with its two-beam advantage, because the two-beam system is only available for separation angles between 0.°3 and 2.°2. The observations were conducted at 22 GHz with a 512 MHz wide recording mode (i.e., a recording rate of 2 Gbps with two-bit quantization) with left-handed circular polarization.

Figure 1 presents the 300 d long light curves from MJD 59100 for the hard (15–50 keV) and soft (2–4 keV) X-ray monitoring showing the two epochs of the KaVA observations, taken from the Swift/BAT[1] and the MAXI[2] mission, respectively. In figure 1, a MAXI count rate of 0.1 photons cm^{-2} s^{-1} is known to be the threshold emission level corresponding to the hard-to-soft state transition, equivalent to the RXTE/ASM[3] 3–5 keV pivotal rate of 3 counts s^{-1} identified by Szostek, Zdziarski, and McCollough (2008) (e.g., Corbel et al. 2012). The first epoch was observed at around a transition state from the soft to hard state in X-rays when the Swift/BAT flux of Cygnus X-3 is at $\lesssim$0.02 counts cm^{-2} s^{-1}. Although there were no observations reported for other wavelengths besides the monitoring data of Swift and MAXI, it could be a minor flaring state, which might be emitted dominantly from a core. Also, for the second epoch, according to Piano et al. (2021a, 2021b) Cygnus X-3 was in its quenching state with no jet-like structure seen before major flaring (Szostek et al. 2008; Koljonen et al. 2010). Therefore, the KaVA observations were most likely carried out in a state without major flaring activity, which has a distinct component from the core.

2.2 VLBI data analysis

After collecting the observed KaVA data from all of the three sites in the KVN and the four sites in the VERA, the data correlation processing was carried out at the Korea–Japan Correlation Center (KJCC) in the Korea Astronomy and Space Science Institute (KASI) located in Daejeon, Korea. In the process of correlation, the 512-MHz band was correlated to form 512 channels with a 1 MHz spacing. The data analyses for calibration and image processing were performed using the National Radio Astronomy Observatory (NRAO) Astronomical Image Processing System (AIPS, e.g., 31DEC18; van Moorsel et al. 1996).

After the bandpass calibration, the amplitude calibration was performed. In this process, the system noise temperatures including atmospheric attenuation, which is sensitive to weather conditions and the elevation angle of the observed source, were measured with the chopper-wheel method (Ulich & Haas 1976). Based on the measured system noise temperatures and gain curves referring to the East Asian VLBI Network (EAVN) status report 2020B,[4] the amplitude calibration was performed with the AIPS task APCAL.

For the phase calibration, we referred to previous VERA astrometric papers (e.g., Nagayama et al. 2020) in which an inaccurate delay model used in the KJCC correlation was replaced with the Earth orientation parameter "EOP 08 C04" (IAU1980; see "The combined solution C04 for Earth Orientation Parameters consistent with International Terrestrial Reference Frame 2008" by C. Bizouard & D. Gambis[5]), the station coordinates of KaVA measured by Geodetic VLBI observations at *K*-band (the project's internal code v2005trf14; Jike et al. 2018), ionospheric delays (CODE's GIM[6]), and zenith wet delays measured with GPS and Japan Meteorological Agency (JMA) meso-scale analysis data for numerical weather prediction[7] for VERA and KVN, respectively. Note

[1] ⟨https://swift.gsfc.nasa.gov/results/transients/CygX-3/⟩.
[2] ⟨http://maxi.riken.jp/star_data/J2032+409/J2032+409.html⟩.
[3] ⟨http://xte.mit.edu/ASM_lc.html⟩.
[4] ⟨https://radio.kasi.re.kr/status_report/files/status_report_EAVN_2020B.pdf⟩.
[5] ⟨https://hpiers.obspm.fr/iers/eop/eopc04_08/C04.guide.pdf⟩.
[6] ⟨http://aiuws.unibe.ch/ionosphere/⟩.
[7] ⟨https://www.jma.go.jp/jma/jma-eng/jma-center/nwp/outline2019-nwp/index.htm⟩.

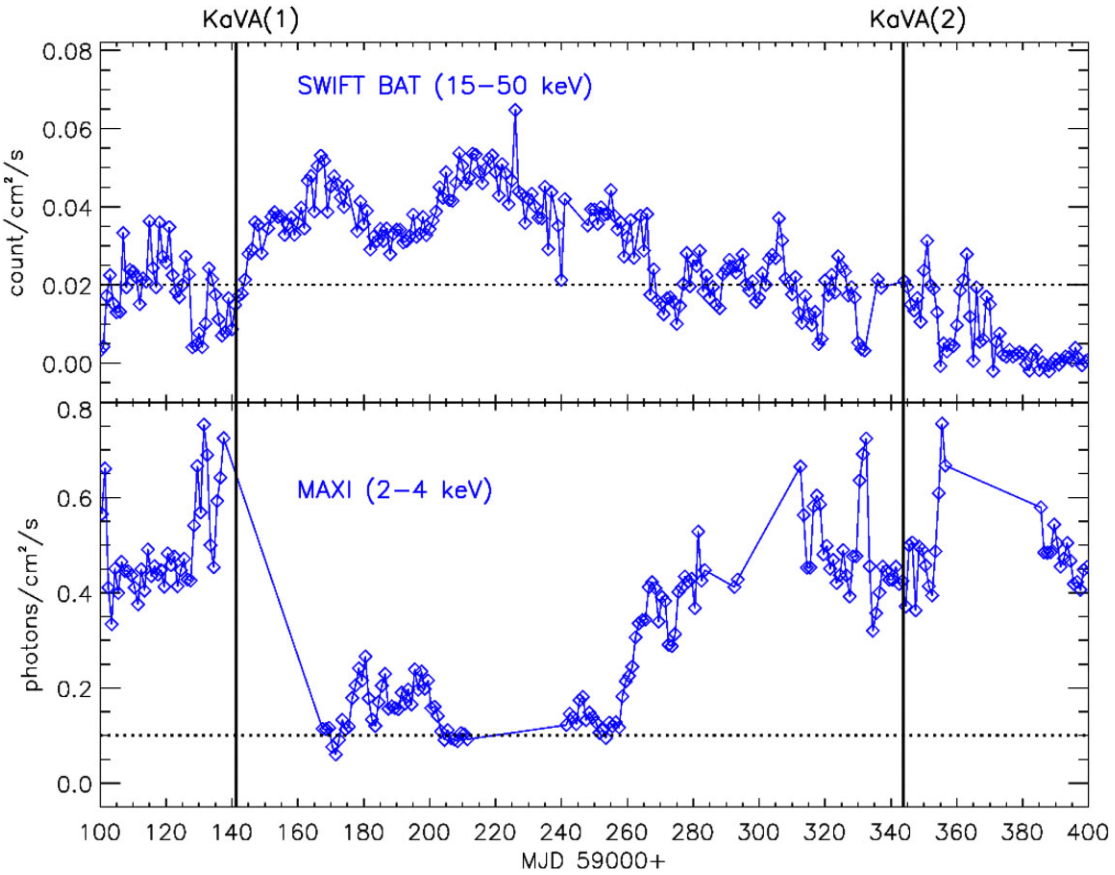

Fig. 1. Daily-averaged X-ray light curves from 2020 September 8 to 2021 July 5. The hard (15–50 keV) and soft (2–4 keV) X-ray data are taken from the Swift Burst Alert Telescope (BAT) all-sky hard X-ray survey (upper panel) and the Monitor of All-sky X-ray Image (MAXI) mission (lower panel), respectively. Cygnus X-3 is typically in its state with short flaring activity when the Swift/BAT flux is near or lower than 0.02 counts cm^{-2} s^{-1}, as shown by the horizontal dotted line in the top panel. The horizontal dotted line in the bottom panel denotes the critical emission level distinguishing the transition from the hard to soft X-ray state, corresponding to the pivotal count rate of 3 counts s^{-1} at 3–5 keV observed with the Rossi X-Ray Timing Explorer (RXTE) All-Sky Monitor (ASM) mission (Corbel et al. 2012; Szostek et al. 2008). The two vertical lines indicate the two observational epochs performed with the KaVA on 2020 October 19 (MJD 59141) and 2021 May 9 (MJD 59343), as designated by KaVA(1) and KaVA(2), respectively. Cygnus X-3 would be in its soft state at the time of the KaVA observations.

that the JMA data cover all the KVN stations, and Nagayama et al. (2015) argued that an accuracy of tropospheric calibration can be achieved within ∼2 cm in both cases of GPS and JMA.

Fringe information of the bandpass calibrator, J2015+4032, was used to calibrate the group delay, rate, and clock offset. These calibration results were then applied to both the target and the phase reference source, J2007+4029. As the next step in the phase calibration, a phase solution of J2007+4029 after fringe search was applied to Cygnus X-3 for measuring the core position of Cygnus X-3 relative to the phase reference calibrator. The phase-referenced image of Cygnus X-3 is shown in figure 2.

2.3 Proper motion

We carried out an elliptical Gaussian fit to the phase-referenced images using the AIPS task JMFIT for each epoch of KaVA observations. The measured core positions and the corresponding errors of Cygnus X-3 are given at the bottom of table 1. In the table, we also adopt the core positions measured by Miller-Jones et al. (2009), Tudose et al. (2007), and Reid and Miller-Jones (2023). Note that the position errors of KaVA observations are formal errors of the elliptical Gaussian fit, and those are underestimates due to systematic errors as indicated by the imperfect convergence on phase-referenced images (see figure 2). Based on figure 2, we assume that systematic errors in (RA, Dec) are (3, 2) and (2, 1) mas for the first and second KaVA astrometric results, respectively. As the phase reference J2033+4000 is only observed by Reid and Miller-Jones (2023) in table 1, the position error of J2033+4000, (4.52, 2.97) mas in (RA, Dec) by the Radio Fundamental Catalog (Petrov & Kovalev 2025) should be considered for the determination of the proper motion of Cygnus X-3 using all available data.

A linear regression fit was performed on all available data using a regress function package of the IDL program by adding the systematic position errors described above in quadrature to the formal errors. The relative weight of individual data refers to the formal and systematic errors. As a result, we measured Cygnus X-3's proper motions with a time baseline of ∼38 yr. The fitting gives the proper motions in RA (α) and Dec (δ) of

$$\mu_\alpha \cos\delta = -2.720 \pm 0.019 \,\mathrm{mas\,yr^{-1}} \quad (1)$$

$$\mu_\delta = -3.693 \pm 0.019 \,\mathrm{mas\,yr^{-1}}, \quad (2)$$

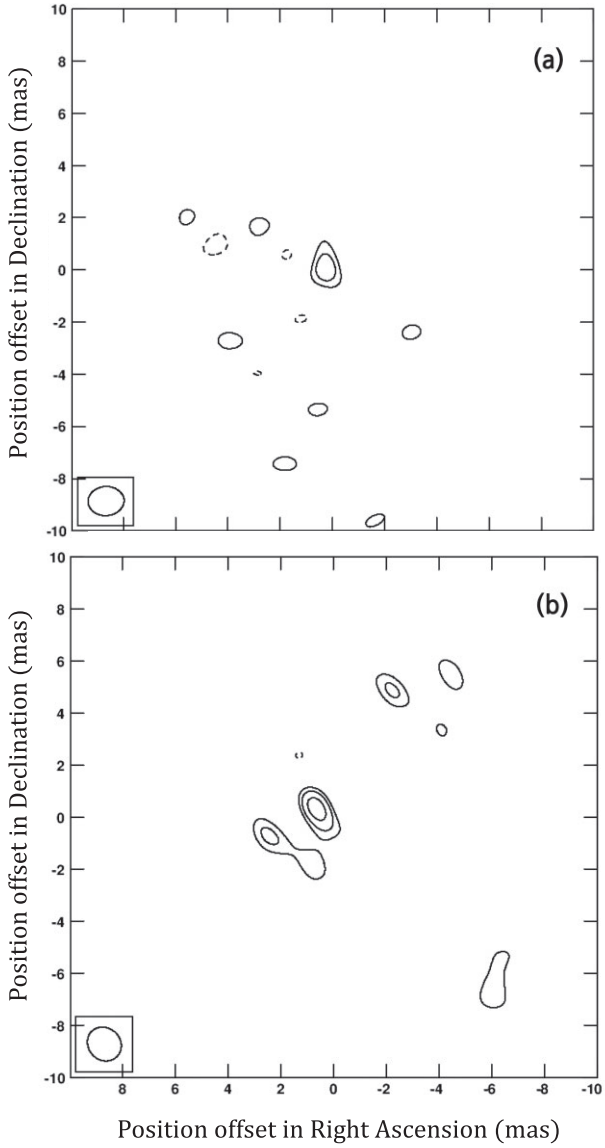

Fig. 2. Contour images of Cygnus X-3 at 22 GHz obtained with the KaVA observations. (a) First observational image on 2020 October 19. The lowest contour level, corresponding to 39.5 mJy, represents a signal-to-noise ratio of 3σ. The synthesized beam size is 1.37×1.11 mas^2 at a position angle of $-81°$. The contour levels are -39.5, 39.5, and 55.3 mJy. (b) Second observational image on 2021 May 9. The lowest contour level, corresponding to 5.8 mJy, represents a signal-to-noise ratio of 3σ. The synthesized beam size is 1.36×1.22 mas^2 at a position angle of 42°.0. The contour levels are -5.8, 5.8, 8.1, and 11.6 mJy. The subsequent contour levels of the images are scaled by factors of -1, 1, 1.4, and 2, respectively.

and a reference position on 2020 January 01 (MJD 58849.0) of $20^{\rm h}32^{\rm m}25\overset{\rm s}{.}7683$ and $+40°57'27\overset{''}{.}8771$ (J2000.0). Note that the errors of proper motions are reliable because the errors are scaled so that the reduced chi-square becomes unity. Our results are consistent with previous results of $(\mu_\alpha \cos\delta, \mu_\delta) = (-2.73 \pm 0.06, -3.70 \pm 0.06)$ mas yr^{-1} based on 25 yr of astrometric results (Miller-Jones et al. 2009). Furthermore, our proper motion results in RA and Dec can be transformed into galactic longitude (l) and galactic latitude (b) following the presented method by Poleski (2013), as shown below:

$$\mu_l \cos b = -4.587 \pm 0.027 \,\mathrm{mas\,yr^{-1}} \quad (3)$$

$$\mu_b = -0.001 \pm 0.004 \,\mathrm{mas\,yr^{-1}}. \quad (4)$$

Figure 3 shows a linear regression fit to all the published core positions, together with the position measured from the KaVA observations, over a span of 38 yr. Furthermore, because measuring the trigonometric parallax is the most reliable way to determine the distance to X-ray binaries, we tried to simultaneously measure the parallax (π) and proper motion components of Cygnus X-3 using the same data. The results of weighted least squares are $(\pi, \mu_\alpha \cos\delta, \mu_\delta) = (-0.160 \pm 0.116$ mas, -2.746 ± 0.035 mas yr^{-1}, -3.697 ± 0.031 mas yr^{-1}). Under a fixed parallax of $\pi = 0.1034$ mas (Reid & Miller-Jones 2023), corresponding to a distance of 9.67 kpc, the results of the proper motion are $(\mu_\alpha \cos\delta, \mu_\delta) = (-2.708 \pm 0.032, -3.694 \pm 0.032)$ mas yr^{-1}. The proper motion results discussed above are in good agreement with each other, regardless of whether the trigonometric parallax is taken into account.

However, we could not measure the trigonometric parallax of Cygnus X-3 because of the large uncertainty in the core shifts for the phase reference calibrator and/or for the target source, which is different along with the different frequencies from 5 to 43 GHz, and because there is no single absolute reference frame for all the individual observations. In addition, the high scattering towards Cygnus X-3 means that the astrometry can be carried out only at high enough frequencies because the scatter-broadened resolution is too low at lower frequencies.

2.4 Peculiar velocity

We calculated the peculiar motion (i.e., non-circular motion) value of Cygnus X-3 using the source parameters—that is, the measured proper motion, the distance (d), the radial velocity (γ) of the mean systemic velocity, and coordinates in J2000.0—as well as the Galactic and solar parameters. The detail of the calculation is summarized in the appendix of Reid et al. (2009). We adopted $\gamma = 208^{+113}_{-127}$ km s^{-1} (Koljonen & Maccarone 2017; Hanson et al. 2000) and $d = 9.67$ kpc for Cygnus X-3 (Reid & Miller-Jones 2023).

For the Galactic and solar parameters, we referred to the A5 model of Reid et al. (2019) where the Galactic constants of ($R_0 = 8.15$ kpc, $\Theta_0 = 236$ km s^{-1}), a universal rotation curve, and solar motion values of ($U_\odot = 10.6$ km s^{-1}, $V_\odot = 10.7$ km s^{-1}, $W_\odot = 7.6$ km s^{-1}) were adopted. The error in the peculiar motion was estimated by considering errors on the proper motion, distance, and systemic radial velocity; see the details in the appendices of Sakai et al. (2020, 2015).

As a result, the components of the peculiar velocity for Cygnus X-3 were determined to be $U_s = -201 \pm 91$ km s^{-1}, $V_s = 212 \pm 89$ km s^{-1} and $W_s = 10 \pm 2$ km s^{-1} at $9.67^{+0.53}_{-0.48}$ kpc, where U_s, V_s, and W_s are positive toward the Galactic Center, the Galactic rotation, and the North Galactic Pole, respectively. Note that (U_s, V_s, W_s) is the residual relative to the universal rotation curve.

3 Discussion

3.1 Debate on the peculiar velocity of the compact star in Cygnus X-3

The peculiar velocity of an X-ray binary, which includes a BH or an NS, is influenced by the kick velocity at the time of compact object formation. This velocity varies along the system's

Table 1. List of astrometric results for Cygnus X-3.*,†,‡

Date	MJD	RA (20^h32^m:ss)	ΔRA (ms)	Dec ($+40°57'$:ss)	ΔDec (mas)	ν (GHz)	Phase reference	Array	Ref.
(1)	(2)	(3)	(4)	(5)	(6)	(7)	(8)	(9)	(10)
1983/09/15	45592.16	25.77697	1.74	28.010929	20.02	22	J2007+4029	VLA	[1]
	45592.17	25.77661	1.74	28.013229	20.01	15	J2007+4029	VLA	[1]
1985/02/05	46101.71	25.77708	1.74	28.008529	20.02	15	J2007+4029	VLA	[1]
	46101.71	25.77635	1.74	28.009929	20.02	22	J2007+4029	VLA	[1]
1987/08/28	47035.33	25.77670	1.75	28.001929	20.14	22	J2007+4029	VLA	[1]
	47035.33	25.77575	1.74	28.004029	20.02	15	J2007+4029	VLA	[1]
1994/03/04	49415.52	25.773962	1.74	27.96544	20.01	22	J2007+4029	VLA	[1]
1997/01/10	50458.94	25.77451	0.87	27.971403	10.01	8	J2007+4029	VLA	[1]
	50458.95	25.77443	1.74	27.974003	20	15	J2007+4029	VLA	[1]
	50458.95	25.77412	1.74	27.974603	20	22	J2007+4029	VLA	[1]
1997/02/08	50487.81	25.773683	0.47	27.961526	2.53	15	J2025+3343	VLBA	[1]
1997/02/11	50490.50	25.773825	0.004	27.9614	0.05	15	J2025+3343	VLBA	[1]
	50490.81	25.773725	0.47	27.961702	2.53	15	J2025+3343	VLBA	[1]
1997/02/22	50501.72	25.773632	0.47	27.961361	2.54	15	J2048+4310	VLBA	[1]
2000/10/20	51837.16	25.773251	0.87	27.934542	10.01	8	J2007+4029	VLA	[1]
	51837.17	25.773837	1.74	27.943713	20	45	J2007+4029	VLA	[1]
	51837.17	25.773651	1.74	27.938742	20.01	15	J2007+4029	VLA	[1]
	51837.17	25.773751	1.74	27.943742	20	22	J2007+4029	VLA	[1]
2001/09/18	52170.21	25.772054	0.48	27.952778	2.66	5	J2052+3635	VLBA	[1]
2002/01/25	52299.76	25.772608	1.74	27.945883	20.01	15	J2007+4029	VLA	[1]
	52299.76	25.772497	1.74	27.941937	20	45	J2007+4029	VLA	[1]
2002/02/15	52320.50	25.77252	0.004	27.9439	0.05	43	J2007+4029	VLBA	[1]
2003/06/08	52798.60	25.772198	0.87	27.939483	10.02	8	J2007+4029	VLA	[1]
2004/01/11	53015.80	25.77206	0.004	27.9362	0.05	15	J2007+4029	VLBA	[1]
2004/09/13	53261.14	25.771848	0.87	27.934083	10.01	8	J2007+4029	VLA	[1]
	53261.16	25.772015	1.74	27.934977	20.02	45	J2007+4029	VLA	[1]
2004/10/17	53295.10	25.77195	0.004	27.9328	0.05	15	J2007+4029	VLBA	[1]
	53295.10	25.771932	0.004	27.93309	0.05	15	J2007+4029	VLBA	[1]
2004/11/21	53330.90	25.771877	0.004	27.93276	0.05	15	J2007+4029	VLBA	[1]
	53330.90	25.771856	0.004	27.93292	0.05	15	J2007+4029	VLBA	[1]
2005/02/06	53407.68	25.772128	0.88	27.932683	10.01	8	J2007+4029	VLA	[1]
2005/06/10	53531.40	25.77191	0.004	27.93043	0.05	15	J2015+3710	VLBA	[1]
2005/12/28	53732.90	25.771673	0.004	27.92944	0.05	15	J2015+3710	VLBA	[1]
2006/02/06	53772.78	25.771998	0.87	27.928083	10.01	8	J2007+4029	VLA	[1]
	53772.79	25.771676	1.74	27.925543	20	45	J2007+4029	VLA	[1]
2006/04/20	53845.50	25.771441	0.2	27.927886	2.7	5	J2007+4029	EVN	[2]
2006/05/18	53873.50	25.771529	0.2	27.929886	2.7	5	J2007+4029	EVN	[2]
2007/06/25	54276.50	25.771004	0.2	27.922886	2.7	5	J2007+4029	EVN	[1]
2008/04/09	54565.50	25.771004	0.2	27.920886	2.7	5	J2007+4029	EVN	[1]
2008/04/23	54579.50	25.771004	0.2	27.918886	2.7	5	J2007+4029	EVN	[1]
2016/10/21	57682.07	25.769682	2.65E-04‡	27.883702	5.0E-03‡	43	J2033+4000	VLBA	[3]
2016/11/01	57693.41	25.769676	3.53E-04‡	27.883548	7.0E-03‡	43	J2033+4000	VLBA	[3]
2017/04/22	57865.57	25.769585	8.83E-05‡	27.881928	2.0E-03‡	43	J2033+4000	VLBA	[3]
2017/04/28	57871.55	25.769581	5.30E-04‡	27.881841	7.0E-03‡	43	J2033+4000	VLBA	[3]
2017/05/05	57878.53	25.769576	3.53E-04‡	27.881681	5.0E-03‡	43	J2033+4000	VLBA	[3]
2017/05/14	57887.51	25.769573	6.18E-04‡	27.881559	1.0E-02‡	43	J2033+4000	VLBA	[3]
2017/10/25	58051.06	25.769451	2.65E-04‡	27.879854	4.0E-03‡	43	J2033+4000	VLBA	[3]
2017/11/05	58062.03	25.769445	4.41E-04‡	27.879820	7.0E-03‡	43	J2033+4000	VLBA	[3]
2020/10/19	59141.40	25.767871	0.009‡	27.874143	0.09‡	22	J2007+4029	KaVA	[4]
2021/05/09	59343.83	25.767818	0.006‡	27.872293	0.11‡	22	J2007+4029	KaVA	[4]

*The columns show the following: (1) date in yyyy/mm/dd; (2) MJD; (3)–(6) coordinates with uncertainties (J2000.0); (7) observing frequency; (8) phase reference source; (9) array. The references in the final column are as follows: [1] Miller-Jones et al. (2009); [2] Tudose et al. (2007); [3] Reid and Miller-Jones (2023); and [4] this paper.

†The proper motion of J2007 + 4029, the most frequently used reference calibrator, is $\mu_\alpha \cos\delta = -0.118$ mas yr $^{-1}$and $\mu_\delta = 0.042 \pm 0.01$ mas yr $^{-1}$ (Gaia Collaboration 2020).

‡These are statistical (thermal) errors. More reliable position errors (i.e., systematic errors) are discussed in subsection 2.3.

Galactic orbit over time. In the case of Cygnus X-3, it can be assumed that Cygnus X-3, associated with its Wolf–Rayet star, has a lifetime no longer than a few Myr, given that the typical lifetime of a Wolf–Rayet star is known to be less than a few Myr (e.g., Crowther 2007). For this reason, the current peculiar velocity of Cygnus X-3 is likely to have been sustained with a similar magnitude for each component (U, V, and W) after forming its compact star.

Miller-Jones et al. (2009) estimated the proper motion ($\mu_\alpha \cos\delta = -2.73 \pm 0.06$ mas yr^{-1}, $\mu_\delta = -3.70 \pm 0.06$ mas yr^{-1}) of Cygnus X-3 based on archival data available in 2008. They first estimated the peculiar velocity to be 9–250 km s^{-1} at 9–10 kpc. The large uncertainty arises from the unknown systemic radial velocity (they assumed $|\gamma| < 200$ km s^{-1}) at that time, coupled with its uncertain distance. Such ambiguity of the inferred peculiar velocity has

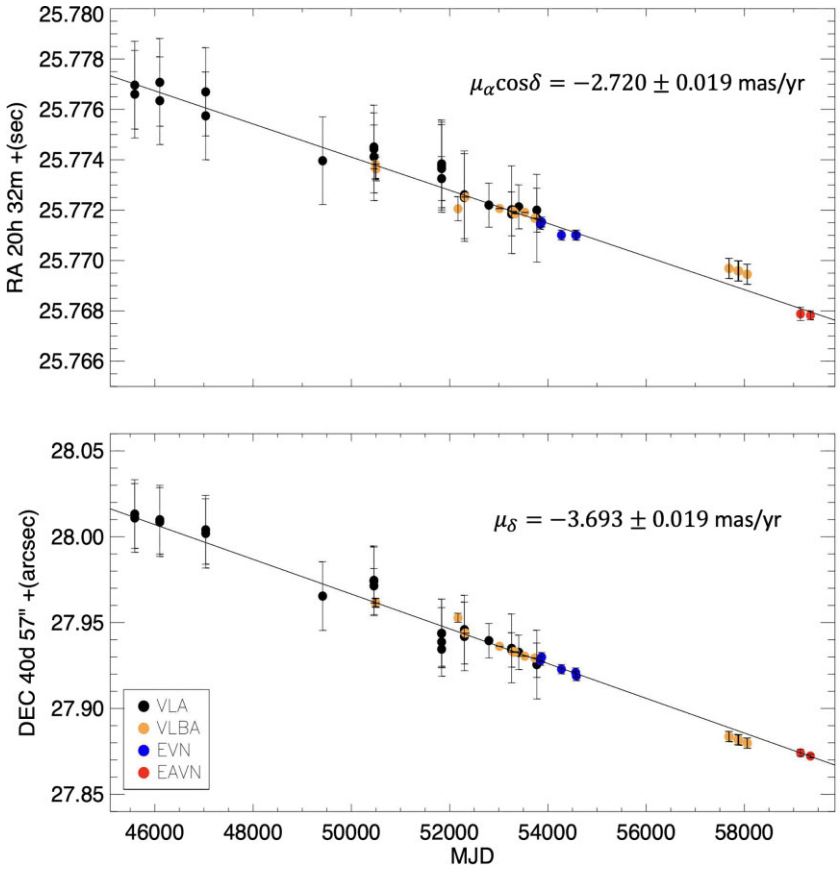

Fig. 3. Proper motion fit for Cygnus X-3 with a time span of 38 yr, in both RA (top panel) and Dec (bottom panel). The solid lines show the best linear regression fits for the proper motions. We assume that the observed positions reported by Reid and Miller-Jones (2023), include the position errors of the phase reference source, and that the first and second KaVA astrometric positions have systematic errors in RA and Dec of (3, 2) and (2, 1) mas, respectively.

made it hard to conclude whether the compact object was formed by a supernova or a failed supernova (i.e., a direct collapse; see, e.g., Mirabel & Rodrigues 2003). Recently, according to Reid and Miller-Jones (2023), considering the $V_{\rm LSR}$ of the star-forming regions near Cygnus X-3, it is suggested that the $V_{\rm LSR}$ of Cygnus X-3 at 9.67 kpc could be approximately $-64\,{\rm km\,s^{-1}}$. This implies that the peculiar velocity of Cygnus X-3 can be lower than $20\,{\rm km\,s^{-1}}$.

However, taking into account the measured proper motion by linear fitting for the interferometry data about 38 yr and the radial velocity from infrared spectroscopy by Koljonen and Maccarone (2017), the estimated peculiar velocity of Cygnus X-3 is $292 \pm 127\,{\rm km\,s^{-1}}$ with 1σ error. This is higher than the peculiar velocities previously estimated by Miller-Jones et al. (2009) and Reid and Miller-Jones (2023), and the peculiar velocity exceeding $100\,{\rm km\,s^{-1}}$ with 1σ error would likely support the system receiving a high natal kick due to an asymmetric supernova explosion. Because different radial velocities were applied to individual estimations, we cannot assert which estimated peculiar velocity has strong robustness. Therefore, the compact star's birth mechanism and physical characteristic in Cygnus X-3 still remain unresolved.

3.2 Comparing the space velocity of Cygnus X-3 with other high-mass X-ray binaries

According to the recent astrometric measurement of the updated distance of Cygnus X-3, the upper limit is determined to be 10.2 kpc (Reid & Miller-Jones 2023). If the upper limit of the distance is adopted, the Wolf–Rayet star mass is estimated to be 11–14 $M_\odot$ using the luminosity–mass relation based on its spectrum (Koljonen & Maccarone 2017). The compact star could be 2.5–3.2 $M_\odot$ because the mass ratio between the compact star and Wolf–Rayet star in Cygnus X-3 is suggested to be 0.23 (Zdziarski et al. 2013). In the NS, the maximum masses in theoretical models and observations for binary systems are $\sim$2.5 and $2.35 \pm 0.17\,M_\odot$, respectively (Rocha et al. 2021; Romani et al. 2022). The theoretical minimum BH mass in an isolated source and close binary are $\sim$4 and $\sim 3\,M_\odot$, respectively. The observed minimum mass of a BH in a detached binary is $\sim 3.3\,M_\odot$ (Thompson et al. 2019). Therefore, the compact star in Cygnus X-3 could be a massive NS near its upper mass limit or a low-mass BH. We cannot define a physical characteristic of the compact object in Cygnus X-3 at present.

Recently, various statistical approaches have been reported, exploring the correlation between the measured peculiar velocity and/or estimated kick velocity and the physical characteristics of binary systems, including NSs and BHs (Gandhi et al. 2019; Atri et al. 2019; Igoshev et al. 2021; Fortin et al. 2022; Zhao et al. 2023). Regarding HMXBs, Fortin et al. (2022) studied the correlation between the estimated kick velocities and the spectral type of companion stars in the HMXBs of NSs (NS-HMXBs). The samples are divided into Be, Oe, and supergiant stars. They found that the mean kick velocity distributions by gamma function for

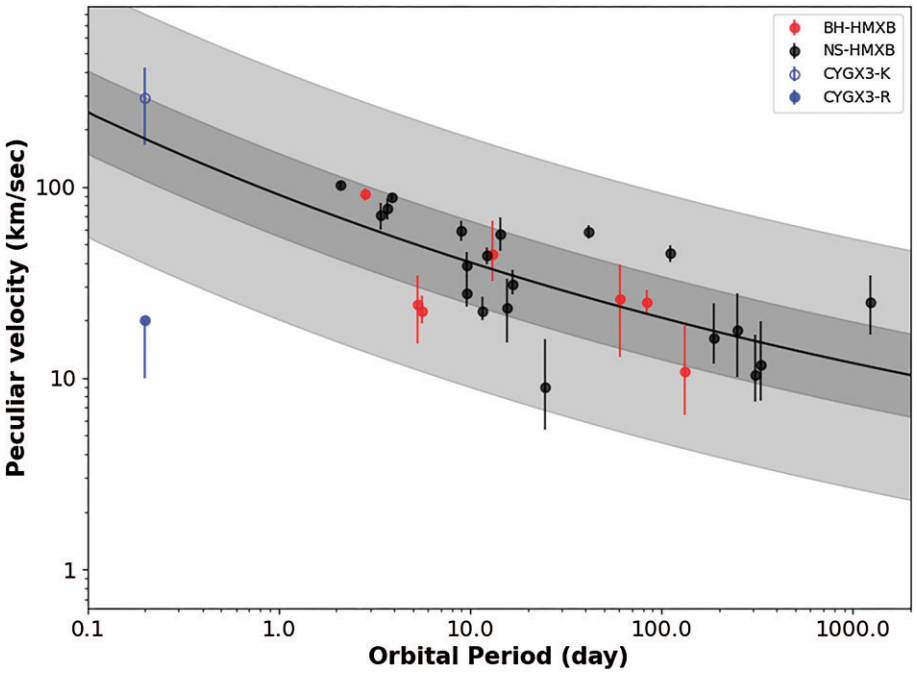

Fig. 4. Distribution of HMXBs in the peculiar velocity–orbital period plane. The black bold line represents the power-law fitting for the peculiar velocity against the orbital period, and dark gray and light gray shaded areas represent the 1σ and 3σ ranges of the fitting, respectively. CYGX3-K and CYGX3-R are represented for peculiar velocities measured in this paper and by Reid and Miller-Jones (2023), respectively.

NS-HMXBs with Be, Oe, and supergiant companions are 91 ± 16, 126^{+39}_{-32}, and 147^{+42}_{-34} km s^{-1}, respectively. It is indicated that NS-HMXBs hosting supergiant stars tend to have higher peculiar velocities than those hosting Be stars. This tendency is also found for the kick velocity distribution between the NS-HMXBs hosting supergiant stars and NS-HMXBs hosting Be stars. Furthermore, using the Python code developed by Atri et al. (2019), Zhao et al. (2023) estimated the potential birth peculiar velocities ($v^{z=0}_{\rm pec}$), supposing that the binaries including a BH or an NS are formed in the Galactic plane.

Zhao et al. (2023) found an anticorrelation between the potential birth peculiar velocities and the total mass ($v^{z=0}_{\rm pec} \propto M^{-0.5}_{\rm tot}$) as well as the orbital period ($v^{z=0}_{\rm pec} \propto P^{-0.2}_{\rm orb}$) when considering all binary samples, including both BH and NS. They adopted the systems involved with HMXBs of BHs (BH-HMXBs) and NS-HMXBs, comprising 7 and 25 samples, respectively, and found no discernible difference in the potential birth peculiar velocities between them.

We compare the tendency of other HMXBs with Cygnus X-3, which could be either BH-HMXBs or NS-HMXBs. We selected samples from the high-mass binary system dataset from Zhao et al. (2023), excluding those lacking information on the mass and orbital period. Consequently, 7 and 20 samples were selected for BH-HMXBs and NS-HMXBs, respectively. According to Zhao et al. (2023), the peculiar velocities of BH-HMXBs and NS-HMXBs are in good agreement with the potential birth peculiar velocity and the correlation results obtained using the peculiar velocity, within a 1σ range, aligned with those derived from the potential birth peculiar velocities (Zhao et al. 2023). Therefore, we investigated the correlation between their present peculiar velocities and the orbital periods as well as total masses of these systems within the sample. Subsequently, we compared the correlation results with the two estimated peculiar velocities for Cygnus X-3 by our method and by Reid and Miller-Jones (2023).

First, regarding the correlation between the total mass and the peculiar velocity for the samples, not including Cygnus X-3, the Pearson correlation coefficient (r) and Spearman correlation coefficient ($r_{\rm S}$) are 0.26 and 0.29, and their p-values are 0.18 and 0.15, respectively. The correlation between peculiar velocity and the total mass is insignificant. Therefore, Cygnus X-3 cannot be compared with the HMXB samples for the relation. However, the correlation coefficient was negative for the sample that included high- and low-mass X-ray binaries (Zhao et al. 2023), in contrast to a positive correlation when the sample is restricted to HMXBs. Therefore, we performed resampling for total mass and peculiar velocity from the 27 sampled objects, generating 10000 random ensembles, each comprising 27 objects. Both the Pearson and Spearman correlations were conducted with each random ensemble. An analysis was conducted to quantify the strength of the correlation, examining the proportion of positive and negative correlations by assessing the sign rates. In this analysis, the rate of the positive correlation coefficient is 100% for the Pearson and Spearman correlations, respectively. Thus, it shows a likely positive correlation between peculiar velocity and total mass, despite the p-values lacking sufficient correlation evidence. Moreover, the positive correlation, increasing peculiar velocity with non-degenerated companion stars' mass in NS-HMXBs, has been previously reported (see figure 3 in Fortin et al. 2022). Therefore, the positive correlation between peculiar velocity and their total mass in HMXB samples, encompassing both BHs and NSs, is likely to have been affected by the NS-HMXB samples.

Second, regarding the correlation between the orbital period and the peculiar velocity, the Pearson correlation coefficient (r) and Spearman correlation coefficient ($r_{\rm S}$ are -0.30 and -0.68, and their p-values are 0.12 and 9.77×10^{-5},

respectively. This shows a significant anticorrelation relation even though the sample was restricted to HMXBs, and the tendency is consistent with the correlation presented by Zhao et al. (2023).

As a result of the robust correlation observed in the Spearman correlation analysis, we performed a power-law fitting for the samples. Figure 4 shows the fitting results and the distribution of peculiar velocities against their orbital periods for the samples, which include the estimated peculiar velocities for Cygnus X-3 presented in this paper and those from Reid and Miller-Jones (2023). The solid line represents the fitting result, with the 1σ and 3σ errors shown by the dark gray and light gray shaded areas, respectively. All samples are located within the 3σ range of the fitting. There is a relationship between the peculiar velocity and the orbital period with $v_{\rm pec} \propto P_{\rm orb}^{-0.09}$. This shows that the peculiar velocity is increased as the orbital period of HMXBs is shortened.

In the case of a 0.2-d orbital period like that of Cygnus X-3, the peculiar velocity would be expected to be $178^{+115}_{-70}\,{\rm km\,s^{-1}}$ within the 1σ range and $178^{+623}_{-139}\,{\rm km\,s^{-1}}$ within the 3σ range, according to the fitting result. Therefore, the high peculiar velocity of Cygnus X-3, $292 \pm 127\,{\rm km\,s^{-1}}$ with the 1σ error in this paper, falls well within the 1σ range of the expected peculiar velocity with a 0.2-d orbital period in HMXBs. This supports the theory that in HMXBs such as Cygnus X-3, if the orbital period is 0.2 d, the peculiar velocity could be $>100\,{\rm km\,s^{-1}}$ with a 1σ range.

According to simulations comparing pre- and post-supernova expansion in HMXBs, it is suggested that even after a supernova, the system's velocity increases as the orbital period of HMXBs becomes shorter (Brandt & Podsiadlowski 1995). Hence, the simulation's expectation roughly aligns with our fitting for the peculiar velocity trend along their orbital period.

4 Conclusions

With the KaVA astrometric observations, we have traced the core position of Cygnus X-3 at two epochs with a half-year interval. Combining our results with previous results, we measured the proper motion and the peculiar velocity of Cygnus X-3 to be $(\mu_\alpha \cos\delta, \mu_\delta) = (-2.720 \pm 0.019, -3.693 \pm 0.019)$ mas yr^{-1} and $292 \pm 127\,{\rm km\,s^{-1}}$ at 9.67 kpc, respectively. To compare Cygnus X-3 with other BH-HMXBs and NS-HMXBs with regards to the relationship between their orbital period and present peculiar velocity, we investigated the correlation between the orbital period and present peculiar velocity for HMXBs. Our analysis revealed a significant anticorrelation, indicating that the peculiar velocity increases as the orbital period of HMXBs shortens. The peculiar velocity measured for Cygnus X-3 appears to align closely with the expected peculiar velocity derived from the fitting result for the relationship between the orbital period and peculiar velocity in HMXBs.

The peculiar velocity range of Cygnus X-3 is debated due to uncertainties in its radial velocity. Thus, we could not rule out the possibility that Cygnus X-3 has a lower peculiar velocity of less than $50\,{\rm km\,s^{-1}}$, which implies a compact star formed by direct collapse. Nonetheless, given the established correlation between the peculiar velocity and orbital period for HMXBs, it is plausible to infer that the compact star in Cygnus X-3 may have experienced a significant natal kick, likely imparted by a supernova explosion.

Funding

This work was supported by the National Research Foundation of Korea (NRF) Grant, which is funded by the Korean Ministry of Science, ICT and Future Planning (MSIP; No. 2016R1A5A1013277), and the National Natural Science Foundation of China (NSFC) Grant No. 11988101. KH has been supported by the Basic Science Research Program through the NRF funded by the Ministry of Education (2016R1A5A1013277 and 2020R1A2C1007219), and in part by the National Science Foundation (NSF) under Grant numbers NSF PHY-1748958 and NSF PHY-2309135 to the Kavli Institute for Theoretical Physics (KITP). KH has been also financially supported during the research year of Chungbuk National University in 2021.

Acknowledgments

We thank all KVN and VERA members who helped operate the array and the Korea–Japan Correlation Center members for correlating wide-band recording data. K.H. acknowledges the Institute for Theory and Computation, Harvard-Smithsonian Center for Astrophysics, for the warm hospitality during the sabbatical year.We are very grateful to Professor J. C. A. Miller-Jones for kindly providing his data, carefully reading our draft, and offering exhaustive and valuable comments.

References

Atri, P., et al. 2019, MNRAS, 489, 3116
Bhargava, Y., et al. 2017, ApJ, 849, 141
Brandt, N., & Podsiadlowski, P. 1995, MNRAS, 274, 461
Corbel, S., et al. 2012, MNRAS, 421, 2947
Crowther, P. A. 2007, ARA&A, 45, 177
Egron, E., et al. 2017, MNRAS, 471, 2703
Fermi LAT Collaboration. 2009, Science, 326, 1512
Fortin, F., García, F., Chaty, S., Chassande-Mottin, E., & Simaz Bunzel, A. 2022, A&A, 665, A31
Gaia Collaboration 2020, VizieR Online Data Catalog, I/350
Gandhi, P., Rao, A., Johnson, M. A. C., Paice, J. A., & Maccarone, T. J. 2019, MNRAS, 485, 2642
Giacconi, R., Gorenstein, P., Gursky, H., & Waters, J. R. 1967, ApJ, 148, L119
Gregory, P. C., Kronberg, P. P., Seaquist, E. R., Hughes, V. A., Woodsworth, A., Viner, M. R., & Retallack, D. 1972, Nature, 239, 440
Hanson, M. M., Still, M. D., & Fender, R. P. 2000, ApJ, 541, 308
Igoshev, A. P., Chruslinska, M., Dorozsmai, A., & Toonen, S. 2021, MNRAS, 508, 3345
Jike, T., Manabe, S., & Tamura, Y. 2018, J. Geodetic Soc. Jpn., 63, 193
Kim, J-S., Kim, S-W., Kurayama, T., Honma, M., Sasao, T., & Kim, S. J. 2013, ApJ, 772, 41
Koch-Miramond, L., Ábrahám, P., Fuchs, Y., Bonnet-Bidaud, J.-M., & Claret, A. 2002, A&A, 396, 877
Koljonen, K. I. I., Hannikainen, D. C., McCollough, M. L., Pooley, G. G., & Trushkin, S. A. 2010, MNRAS, 406, 307
Koljonen, K. I. I., & Maccarone, T. J. 2017, MNRAS, 472, 2181
Miller-Jones, J. C. A., Blundell, K. M., Rupen, M. P., Mioduszewski, A. J., Duffy, P., & Beasley, A. J. 2004, ApJ, 600, 368
Miller-Jones, J. C. A., Sakari, C. M., Dhawan, V., Tudose, V., Fender, R. P., Paragi, Z., & Garrett, M. 2009, in Proc. Science and Technology of Long Baseline Real-Time Interferometry: The 8th International e-VLBI Workshop, PoS(EXPReS09) (Trieste: SISSA), 17
Mioduszewski, A. J., Rupen, M. P., Hjellming, R. M., Pooley, G. G., & Waltman, E. B. 2001, ApJ, 553, 766
Mirabel, I. F., & Rodrigues, I. 2003, Science, 300, 1119

Mori, M., et al. 1997, ApJ, 476, 842
Nagayama, T., et al. 2015, PASJ, 67, 65
Nagayama, T., et al. 2020, PASJ, 72, 52
Ogley, R. N., Bell Burnell, S. J., & Fender, R. P. 2001, MNRAS, 322, 177
Petrov, L. Y., & Kovalev, Y. Y. 2025, ApJS, 276, 38
Piano, G., et al. 2021a, Astronomer's Telegram, 14662, 1
Piano, G., et al. 2021b, Astronomer's Telegram, 14780, 1
Poleski, R. 2013, arXiv:1306.2945
Reid, M. J., et al. 2009, ApJ, 700, 137
Reid, M. J., et al. 2019, ApJ, 885, 131
Reid, M. J., & Miller-Jones, J. C. A. 2023, ApJ, 959, 85
Rocha, L. S., Bachega, R. R. A., Horvath, J. E., & Moraes, P. H. R. S. 2021, arXiv:2107.08822
Romani, R. W., Kandel, D., Filippenko, A. V., Brink, T. G., & Zheng, W. 2022, ApJ, 934, L17
Sakai, N., et al. 2015, PASJ, 67, 69
Sakai, N., et al. 2020, PASJ, 72, 53
Szostek, A., Zdziarski, A. A., & McCollough, M. L. 2008, MNRAS, 388, 1001
Tavani, M., et al. 2009, Nature, 462, 620
Thompson, T. A., et al. 2019, Science, 366, 637
Trushkin, S., McCollough, M., Nizhelskij, N., & Tsybulev, P. 2017, Galaxies, 5, 86
Tudose, V., et al. 2007, MNRAS, 375, L11
Ulich, B. L., & Haas, R. W. 1976, ApJS, 30, 247
van Kerkwijk, M. H., Geballe, T. R., King, D. L., van der Klis, M., & van Paradijs, J. 1996, A&A, 314, 521
van Moorsel, G., Kemball, A., & Greisen, E. 1996, ASP Conf. Ser., 101, 37
Vanbeveren, D., Mennekens, N., van den Heuvel, E. P. J., & Van Bever, J. 2020, A&A, 636, A99
Wagner, R. M., Kreidl, T. J., Martell, P. J., & Beaver, J. 1990, ASP Conf. Ser., 8, 361
Waltman, E. B., Foster, R. S., Pooley, G. G., Fender, R. P., & Ghigo, F. D. 1996, AJ, 112, 2690
Zdziarski, A. A., Mikolajewska, J., & Belczynski, K. 2013, MNRAS, 429, L104
Zhao, Y., Gandhi, P., Dashwood Brown, C., Knigge, C., Charles, P. A., Maccarone, T. J., & Nuchvanichakul, P. 2023, MNRAS, 525, 1498

Received: 2024 May 21; Accepted: 2025 March 25